Heliyon 9 (2023) e18988

Contents lists available at ScienceDirect

Heliyon

journal homepage: www.cell.com/heliyon

Synthesis, characterization, DFT calculations and biological activity of new Schiff base complexes

Fatmah M. Alkhatib *, Hajar Mubashir Alsulami

Department of Chemistry, Faculty of Applied Science, Umm Al-Qura University, Makkah, P.O. Box 715, Saudi Arabia

ARTICLE INFO

Keywords:
Schiff base
Antitumor activities
DFT method
Molecular docking

ABSTRACT

Schiff bases ligand (**HL**) was produced by condensing 4-aminobenzohydrazide with N-(4-chlorophenyl)-2-(4-formylphenoxy)acetamide. Cobalt (II), nickel (II), and copper (II) acetate and ligand are reacted to form 1:1 complexes. By using electronic spectra, magnetic susceptibility measurements, infrared data from ^{1}H NMR, and XRD studies, the ligand and its metal complexes have been characterized. According to the spectrum data, the ligand functions as a monobasic bidentate, coordinating with the nitrogen atom of azomethine (−C═N−) group and the oxygen atom of carbonyl group in enol form. An octahedral structure has been proposed for Co(II), Ni(II), and Cu(II) complexes according to magnetic and electronic spectrum analysis. Using the DFT method, the computational investigations of the ligand and its metal complexes showed the bond lengths, bond angles, and quantum chemical parameters. To determine the thermal stability and mode of thermal degradation of hydrazone ligand and its complexes, thermogravimetric analysis was approved out on the samples. Two calculated method, Horowitz-Metzger and Coats-Redfern, were used to calculate the characteristics of the composites' thermal degradation mechanisms at each step, including their breakdown kinetics. The ligand and its complexes were investigated for their cytotoxicity *in vitro* compared to human amnion (**WISH**) and epitheliod carcinoma (**Hela**). The Ni(II) complex showed highly inhibition against (**WISH**) growth (IC_{50} = 18.28±1.8 μM) with relationship to the produced chemicals and other common medications. The interaction between the ligand and its complexes with the genetic tumor (3hb5) receptor was examined using docking experiments.

1. Introduction

A lot of people are interested in Schiff bases since they are simple to make and have a wide range of coordination chemistry [1]. By condensing basic amines and carbonyls, Schiff bases are a product of ketones or aldehydes in which the carbonyl group (C═O) has been replaced by an imine or azomethine group (>C═N−) [2]. Among the most popular organic molecules, Schiff bases have a variety of uses, including as pigments and dyes polymer protectors, chemo sensors, and stages in organic synthesis [3].

The acylhydrazone cyclic compounds are a significant class of heterocyclic chemicals with a variety of biological effects [4–6]. The simplicity of synthesis makes it possible to build a variety of chemical libraries for the search for potential bioactive compounds. The double bond between C and N in hydrazones is a factor in the creation of geometric isomers (syn and anti). Isomerism in shape possibly play a key part in bioactivity of hydrazones, so research into it is critical for developing synthetic procedures for the choosy production

* Corresponding author.
E-mail address: fmkhatib@uqu.edu.sa (F.M. Alkhatib).

https://doi.org/10.1016/j.heliyon.2023.e18988
Received 10 May 2023; Received in revised form 21 July 2023; Accepted 4 August 2023
Available online 9 August 2023

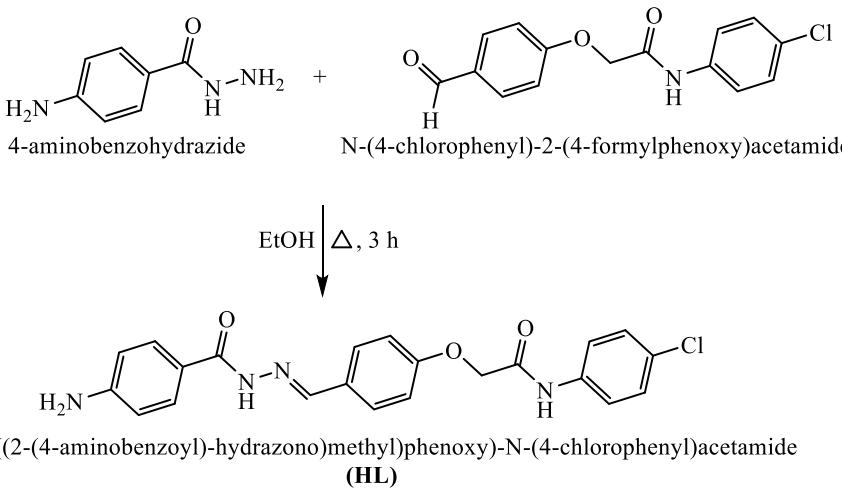

Fig. 1. Synthesis of targeted ligand (**HL**).

of a certain isomer [7]. Comprehensive study into hydrazides and related derivatives has revealed several biological activities in recent years. Some articles reporting the good therapeutic activities of acyl hydrazones were discovered during a literature search. Hydrazones with azometine proton (−NHN═CH−) are a significant class of substances for the development of new drugs. Hydrazide-hydrazones have recently obtained prominence because of their varied biological characteristics, which include antibacterial [8], antifungal [9], and anticonvulsant [10], antiinflammatory, antimalarial, and antituberculosis properties. Numerous series of substituted hydrazide-hydrazone compounds were created and reported in the literature for them in-vitro antibacterial activity against a wide variety of microorganisms. In medical biotechnology, methods based on hydrazone are employed to couple medications to specific antibodies, such as antibodies compared to a specific kind of tumor cell. At pH 7.0, the hydrazone-based connection is stable (in the blood), but it dissolves quickly in the acidic atmosphere of the cell's lysosomes. As a result, the medicine is dispersed into the cell, that it performs its role [11]. Hydrazides have been employed as electron acceptors as well in analytical chemistry [12]. Various effective compounds, such as iproniazide and isoniazide, are as anti-tubercular medications [13,14].

The coordination complexes of hydrazones have attracted particular interest because of their complicated hydrazone structural makeup, electrochemical potential, and magnetic properties [15,16]. They are a physiologically significant metal, and their hydrazone complexes have fascinating biological properties such bacteriostatic activity [17], efficient DNA binding [18] also anti-microbial [19, 20] among others.

Given the aforementioned uses, it was deemed worthwhile to synthesize and describe 2-(4-((2-(4-aminobenzoyl)-hydrazono) methyl)phenoxy)-*N*-(4-chlorophenyl) acetamide (**HL**) and its Co(II), Ni(II) and Cu(II) metal complexes (**1**–**3**). In vitro cytotoxic activity against Epitheliod Carcinoma (**Hela**) and Human Amnion (**WISH**) was examined using the ligand's interaction with metal ions, and the results were compared to the ligand's uncoordinated form. Studies on computer modelling of molecules were too conducted. According to the molecular docking data, the mutant (3hb5) protein for malignancy prefers to connect with **HL** and its Co(II), Ni(II), and Cu(II) complexes (**1–3**).

2. Experimental

2.1. Chemicals and Equipment's

Each of the chemicals from Aldrich and Fluka were purchased and used without further purifying. All the equipment applied has been recently explained [21,22].

2.2. Ligand preparation

A suspension of 4-aminobenzohydrazide (1.51, 10 mmol) and *N*-(4-chlorophenyl)-2-(4-formylphenoxy)acetamide (2.89, 10 mmol) was refluxed in ethanol for 3 h to achieve the condensation at the more nucleophilic nitrogen of hydrazide (-CONHNH$_2$). The generated substance upon cooling was gathered to give the targeted ligand, 2-(4-((2-(4-aminobenzoyl)-hydrazono)methyl)phenoxy)-*N*-(4-chlorophenyl) acetamide (**HL**) (Fig. 1). The structure of entire new ligand was checked via Infra-red and ^{1}H NMR which were in full favor with the assigned molecular structure.

Table 1
The ligand's (**HL**) physical characteristics and elemental assessments, as well as those of its complexes (**1**–**3**).

Structure (Molecular Formula)	Mol. Weight	M.P. (°C)	Yield (%)	Color	Found (Calcd.) (%)				Λ_M Ω^1 cm^2 mol^{-1}	μ_{eff} B. M.
					C	H	N	M		
$C_{22}H_{19}ClN_4O_3$ (HL)	422.87	241	76	White	**62.61 (62.49)**	**4.48 (4.53)**	**13.32 (13.25)**	–	–	–
$C_{24}H_{27}ClCoN_4O_8$ **(1) [Co(L) $(CH_3COO)(OH_2)_2$]** H_2O	593.88	**> 300**	71	Brown	**50.43 (50.06)**	**4.14 (4.38)**	**9.59 (9.73)**	**10.18 (10.23)**	7	4.71
$C_{24}H_{27}ClN_4NiO_8$ **(2) [Ni(L) $(CH_3COO)(OH_2)_2$]** H_2O	593.64	**> 300**	70	Green	**50.14 (50.08)**	**4.30 (4.38)**	**9.67 (9.73)**	**10.28 (10.20)**	15	3.12
$C_{24}H_{27}ClCuN_4O_8$ **(3) [Cu(L) $(CH_3COO)(OH_2)_2$]** H_2O	598.50	**> 300**	73	Green	**49.91 (49.66)**	**4.29 (4.34)**	**9.62 (9.65)**	**10.88 (10.95)**	12	1.75

2.3. The complexes' preparation (1–3)

Complexes of Co(II), Ni(II), and Cu(II) (**1–3**) were made using the usual method [22,23]. A heated ethanol solution of metal acetate (0.02 mol) added dropwise to a molar ratio quantity of the suitable ligand (0.02 mol) in ethanol, and the combination was agitated for 5 min. For 2 h, mixture was refluxed. The colored product that had developed was filtrated, wash away by hot ethanol, also dehydrated by filtering above calcium chloride anhydrous in a desiccator. The separate complexes' There is a list of physical and analytical data. The complexes were determined to be non-electrolytes because the anions' test result was positive after complexes were broken down, informing the coordinating sphere of their presence. The complexes' melting temperature is high and soluble in the majority of conventional organic solvents.

2.4. Computational details

Utilizing the Materials Studio package's DMOL^3 tool, that is proposed to realisation of large-scale (DFT) calculations, we carried out cluster calculations [24]. Calculations for DFT semi-core pseudopods (dspp) were done using double reason groups for numbers and polarization functional theory (DNP). The 6-31G Gaussian basis sets and the DNP foundation sets are of equivalent value [25]. Delley et al. demonstrated that for basis sets of the same size, DNP matrix elements are more correct than Gaussian basis sets [26]. Generalized gradient approximation (GGA)-based RPBE functional [27] is currently the top functional transfer [28] for accounting for the effects of electron exchange and correlation. There are no symmetry restrictions placed on the geometric optimization process.

2.5. Molecular docking

In an experiment to determine the method of synthesized molecular docking was studied. Applying the Molecular Operating Environment tool, all molecular simulation studies were performed (MOE, 2015.10). All possible reductions were made using MOE till automatic determination of the partial charges and an RMSD gradient of 0.05 kcal (mol^{-1} Å^{-1}) with MMFF94x power area [29] were made.

Using the protein data bank, download X-ray crystalline organization of the mutated breast tumor receptor (PDB ID: 3hb5) [30]. Using the Protonate 3D technique in MOE with the defaulting choices, the protein was prepped for the docking research for The protein co-crystallized by eliminating ligands and water molecules that aren't essential to the bond formation Docking was accomplished using the London dG score methodology and the Triangle Matching engine placement approach.

2.6. Biological analysis

2.6.1. Assessment of cytotoxic effects in vitro

HL and its complexes (**1–3**) were investigated for their cytotoxicity against Epitheliod Carcinoma (**Hela**) and Human Amnion (**WISH**) [31]. Holding firm for biological items and vaccinations (VACSERA), Cairo, Egypt, got the cell lines from ATCC on its behalf. The MTT test accustomed to evaluate the restraining effects of substances on cell proliferation in the aforementioned cell lines. Colorimetric method relies on living cells' mitochondrial succinate dehydrogenase to alteration yellow tetrazolium bromide (MTT) into a purple formazan product. In RPMI-1640 media with 10% foetal bovine serum, cell lines were grown. At 37 °C in an incubator with 5% CO_2, antibiotics of 100 units/mL DOX were presented. The cell lines were seeded at a density of 1.0×10^4 cells/well in a 96-well plate for 48 h at 37 °C with 5% CO_2. Following incubated at 37 °C, the cells were exposed to several chemical concentrations and incubated for 24 h. Following a 24-h drug treatment timeframe, 20 μl of a 5-mg/mL MTT solution was applied and incubated for 4 h. Each well receives 100 μL of dimethyl sulfoxide (DMSO) to dissolving the created indigo formazan. Use of a plate reader, the colorimetric analyze is measured and measured at 570 nm of absorbance. (EXL 800, USA). By multiplying (A570 of modified samples by A570 of untreated samples) by 100, the relative cell viability was estimated as a percentage [32].

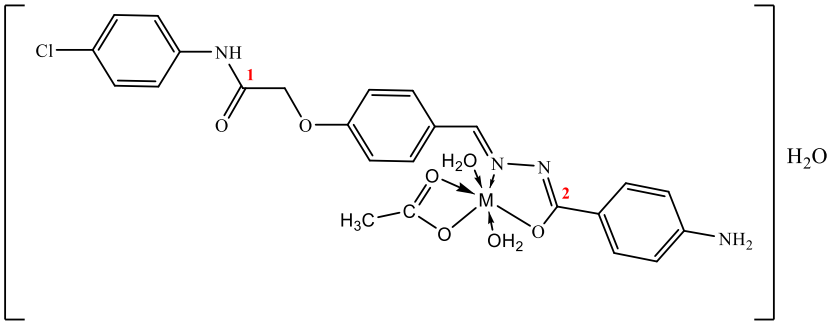

M = Co(II), Ni(II) and Cu(II)

Fig. 2. Structure of the complexes (**1**–**3**).

2.6.2. Antioxidant activity screening assay by ABTS method

The effectiveness of the produced substances at scavenging free radicals was assessed using the ABTS technique [33]. The ABTS chemical was created by combining 88 μL of 140 mM potassium sulphate solution with 5 mL of 7 mM ABTS. The mixture also was diluted by water (1:44, v/v) after being left to generate free radicals at in the dark at room temperature for 16 h 100 μL of ABTS chemical and 100 μL of material were combined in a 96-well microplate to measure the scavenging activity. The mixture was then incubated at room temperature for 6 min. Utilizing an ELISA reader (TECAN, Gröding, Austria) and 100% methanol as a reference, the intensity was assessed at 734 nm after incubating. The below formula was employed to determine the ABTS scavenging result (Eq. (1)):

$$\text{Inhibition } (\%) = \frac{\text{Absorbance of negative control} - \text{Absorbance of tested sample}}{\text{Absorbance of negative control}} \times 10 \quad (1)$$

3. Data and analysis

Table 1 presents elemental study findings as well as several physical characteristics of the ligand (**HL**) and its Co(II), Ni(II), and Cu (II) complexes (**1–3**). They equilibrium in air and are soluble in the majority of conventional organic solvents. The resulting complexes (**1–3**) were measured for molar conductance in DMSO at a concentration of 10^{-3} M and 25 °C. The complexes' non-electrolytic character has measurements for molar conductivity between 7 and 15 $\Omega^1 cm^2 mol^{-1}$ [34,35].

3.1. Spectrum of FTIR and ^1H NMR

Table S1 (Supplementary material) shows Ligand (**HL**) and its metal chelates' most significant infrared bands. The ligand has several coordination sites that resulted in a variety of coordination behaviors. The ligand's and its metal chelates' KBr spectrum show that (**HL**) interacts in the enol form. Two bands in chart of (**HL**) that correspond to $\nu(C{=}N)_{azomethine}$ and (C═C), respectively, can be found at 1593 and 1445 cm^{-1} [36]. The two bands at 1674 and 1700 cm^{-1} are attributable to the vibrations $\nu(C{=}O)^1$ and $(C{=}O)^2$, respectively [37]. The moderate bands at 3406 and 3341 cm^{-1} that $\nu(NH)_{hydrazo}$ and are responsible for (NH) [38] vibrations, respectively. The band designated to ν(N–N) vibration is at 1053 cm^{-1} [38].

The ^1H NMR spectroscopy of (**HL**) in DMSO-d_6 (Fig. S1) (Supplementary material) two stimuli are shown at d = 10.016 and 11.417 ppm of $\nu(NH)_{hydrazo}$ and ν(NH) [36] protons, respectively. a scant signal at 8.16 ppm is caused by azomethine (-CH═N) proton [38]. The pluralities at 7.19–8.00 ppm due to proton phenyl rings [39].

An analysis of the IR of the chelates of title metals (**1–3**) revealed that (**HL**) acts as a monobasic NO bi-dentate ligand by the (C═N) azomethine and $(C{=}O)^2$ carbonyl group (Fig. 1). There is this behaviour across the complexes. This activity is implied by: (i) With the simultaneous development of novel bands attributed to different frequencies (C═N*-N═C) and (C–O) in all metal complexes at (1601 cm^{-1}) and (1174 and 1179) cm^{-1}, respectively, a band for $\nu(C{=}O)^2$ and $(NH)_{hydrazo}$ modes has vanished [39], (ii) Since the band of $\nu(C{=}O)^1$ mode unchanged (1674 cm^{-1}), There is no connection in this group, (iii) coordination via azomethine nitrogen's raising of ν(N–N) to a great wavenumber [40] and (iv) The novel bands at 502–508 and 475–479 cm^{-1} were related to ν(M − O) and (M − N) vibrations, verifying the proposed manner of coordination, respectively [40]. The coordinating acetate absorption spectra for $\nu_{asym}(OCO)$ and $(OCO)_{sym}$ were detected at 1530 and 1510 cm^{-1} and 1465 and 1439 cm^{-1}, respectively. All of the complexes' Δν values (ν_{asym}- ν_{sym}) of (OCO) are much less than 164 cm^{-1} [41], demonstrating OAc's bidentate coordination mode. The hydroxyl group (OH) of water may be responsible for the complexes' strong signal at 3500 cm^{-1} in the IR spectrum. Thermogram will also validate the most recent claim.

3.2. Magnetic data and electronic spectrum

For **HL** and its metal complexes, Nujol mull and DMSO electronic spectra matching to each metal complex were shown (Fig. S2) (Supplementary material). The ligand's spectra shows good band of absorbance at 213 nm (46948 cm^{-1}) for $(C{=}N)_{azomethine}$ π→π*,

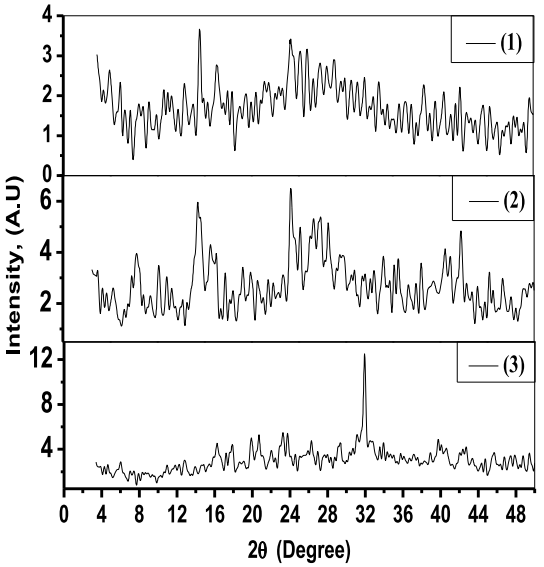

Fig. 3. XRD complexes chart (**1**–**3**).

which changes to greater rates in chelates and supports coordination by the N atom of compound. It is possible to attribute the band at 294 nm (34013 cm^{-1}) to the carbonyl group's (n→π*) transition.

In the **[Co(L)(CH$_3$COO)(OH$_2$)$_2$]** H_2O spectral range show two wide bands are seen at 608 and 647 nm (16447 and 15456 cm^{-1}) for $^4T_{1g}$ (F) →$^4T_{1g}$ (P) (ν_3) and $^4T_{1g}$ (F) →$^4A_{2g}$ (F) (ν_2) octahedral large-spin d^7 transitions [42] (Fig. 2). Additionally, the magnitude of the magnetic moment supports the suggested form (4.71 B M.). The estimated parameters of the ligand site (Dq, B and β) are: 815, 680 and 0.70 cm^{-1}. β decrease in value from 1indicates the metal-ligand bond's covalence [43].

In spectrum of **[Ni(L)(CH$_3$COO)(OH$_2$)$_2$]** H_2O complex (**2**), two bands are shown at 386 and 772 nm (25907 and 12953 cm^{-1}) assignable to the $^3A_{2g}(F) \rightarrow {}^3T_{1g}(F)$ (ν_3) and $^3A_{2g}(F) \rightarrow {}^3T_{1g}(P)$ (ν_2) transitions, respectively, in an octahedral structure [44] (Fig. 2). The ligand field's variables' calculated values (Dq, B and β: 784, 1044 and 1.00 cm^{-1}) in addition to magnetic moment measurements (3.12 B M.) which are octahedral Ni(II) chelates.

In the **[Cu(L)(CH$_3$COO)(OH$_2$)$_2$] H$_2$O** spectral range, In an octahedral situation, two bands are seen at 680 and 424 nm (14706 and 23585 cm^1) that are attributed to the $^2B_{1g} \rightarrow {}^2E_g$ and $^2B_{1g} \rightarrow {}^2A_{1g}$ shifts, respectively. The magnetic moment estimate (1.75 B M.) is consistent with the octahedral surroundings in around Cu(II) ion (Fig. 2). The L→M electron transfer mechanism may be given to the wavelength at 394 nm (25380 cm^{-1}) [45].

3.3. Band gap (Eg) calculations

The assimilation approach involves taking in a photon with recognized energy transitions from one energy state to another. in order to excite an electron. The kind of potential electron transfer is dependent upon the shift in the emission absorbed. Fundamental absorbing is the name for the band-to-band transfer. The Kubelka-Munk method [46] accustomed to determine E_g values in order to translate incorporation of diffuse reflection into the absorption coefficient α (Eq. (2)):

$$\alpha \approx \frac{K}{S} = \frac{(1-R_\infty)^2}{2R_\infty} = F(R_\infty) \tag{2}$$

The coefficients of absorption and scattering in Eq. (1) are K and S, respectively, and is reflecting R_∞ is equal to $R_{sample}/R_{standard}$. Tauc plot was then utilised. This technique presupposes that Eq. (1)'s absorption coefficient can be represented as Eq. (3):

$$\alpha h\nu = \beta\left(h\nu - E_g\right)^m \tag{3}$$

where Eg is the (optical) energy band gap of permitted transitions, A is a material constant, h is the Planck's constant, v is the frequency of light, and γ is the power factor specific to the transition's style. Because transfer is believed to be directly permitted for such substances, it is γ agreed that has a value of 2 [47].

So, by plotting $[\alpha h\nu]^2$ against $h\nu$ where ($\alpha = 2.303/dA$) We may get the optical Eg of the material from the x-axis (α = 0) intercept of the line tangent to the curve's inflection point, where d is the width of the cell and A is the absorbance. This was discovered via using a sigmoidal Boltzmann function to fit the converted Kubelka-Munk equation vs the power of photons. The optical Eg quantity was then calculated using line's x-axis intercept perpendicular to curve's turning point [48].

According to Fig. S3 (Supplementary material), measurements of the direct band gaps (Eg) in chelates of Co(II), Ni(II), and Cu(II) are 2.23, 2.18, and 1.82 eV, respectively. The fact that there is a direct correlation between the value of (Eg) and the atomic number of

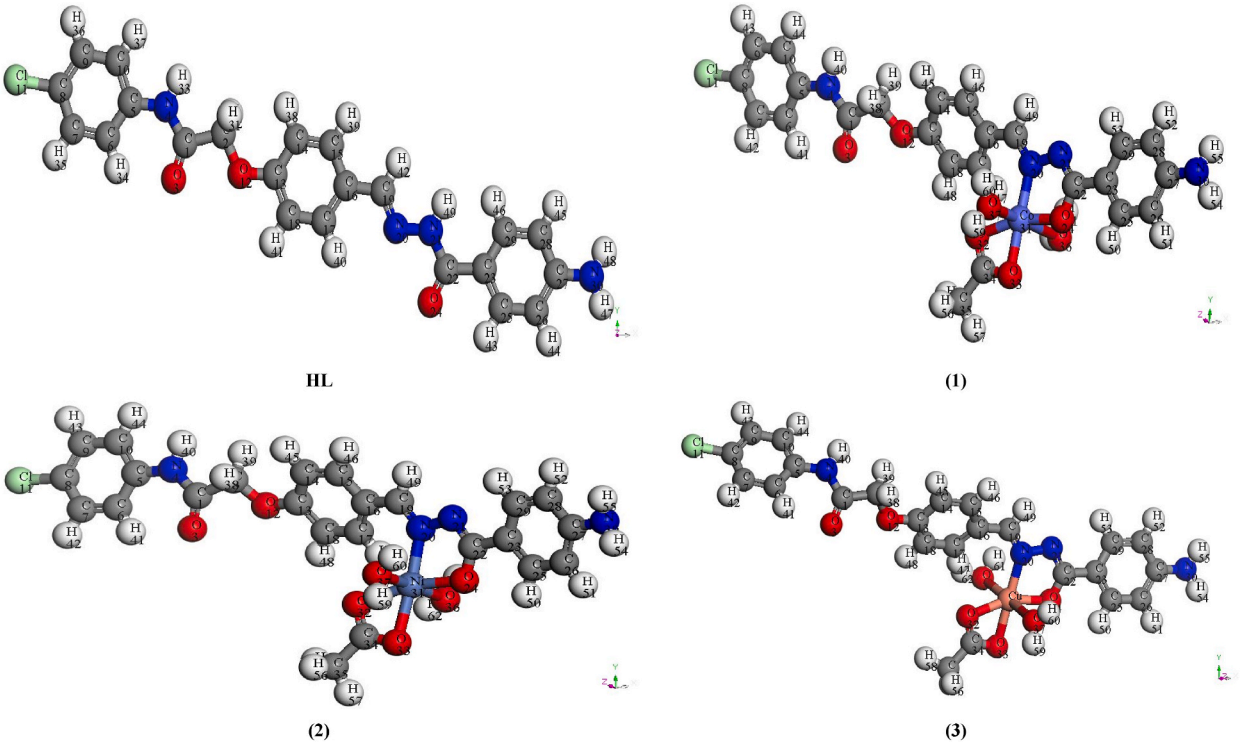

Fig. 4. Chemical compositions of **HL** and its complexes (**1**–**3**).

the nucleus suggests that (Eg) is dependent on electric arrangement of metal ion's d orbits. Band gap measurements place these compounds in the same class as exceptionally effective solar substances and indicate that they are semi-conductors. Consequently, the most recent materials could be considered potential sources for solar energy collection in solar cell applications.

3.4. Diffraction of X-rays

For Co(II), Ni(II), and Cu(II) chelates (**1–3**) (Fig. 3), during powdered X-ray diffraction investigation. The ideal crystal structure and space group for the complexes can be found in Tables S2–S4 (Supplementary material). The crystalline data show that all complexes have the same monoclinic crystallin system. Comparative properties of the crystallin structure and complex structure developed founded on outcomes of various methodologies can be seen throughout the series of complexes.

From the XRD pattern, the average size (Cs) and dislocation density (D) can be calculated as follows: Eqs. (4) and (5) [49].

$$C_s = \frac{0.95\,\lambda}{\beta_{1/2}\,cos\,\theta} \tag{4}$$

$$D = \frac{1}{C_s^2} \tag{5}$$

Where is the angle of diffraction θ, $\beta_{1/2}$ is the full width expressed in radians at the half-maximum standard diffraction pattern, and is wavelength of X-ray radiation (λ = 1.5406 Å) [50].

The ligand's Co(II), Ni(II), and Cu(II) complexes' determined amounts of Cs are observed to be 27.11, 26.27, and 32.16 nm, respectively. The computed amounts of D for ligand and the Co(II), Ni(II), and Cu(II) complexes are 1.36×10^{-3}, 1.45×10^{-3} and 9.66×10^{-4} nm^{-2}, respectively.

3.5. Computational research

3.5.1. DFT-based geometry optimization

Molecules' geometries with **HL** atom sequence and their complexes are shown in the (Fig. 4). The listings (Tables S5–S8) contain information such as bond lengths and angles that verify the recommended structures. The findings included the observations below.

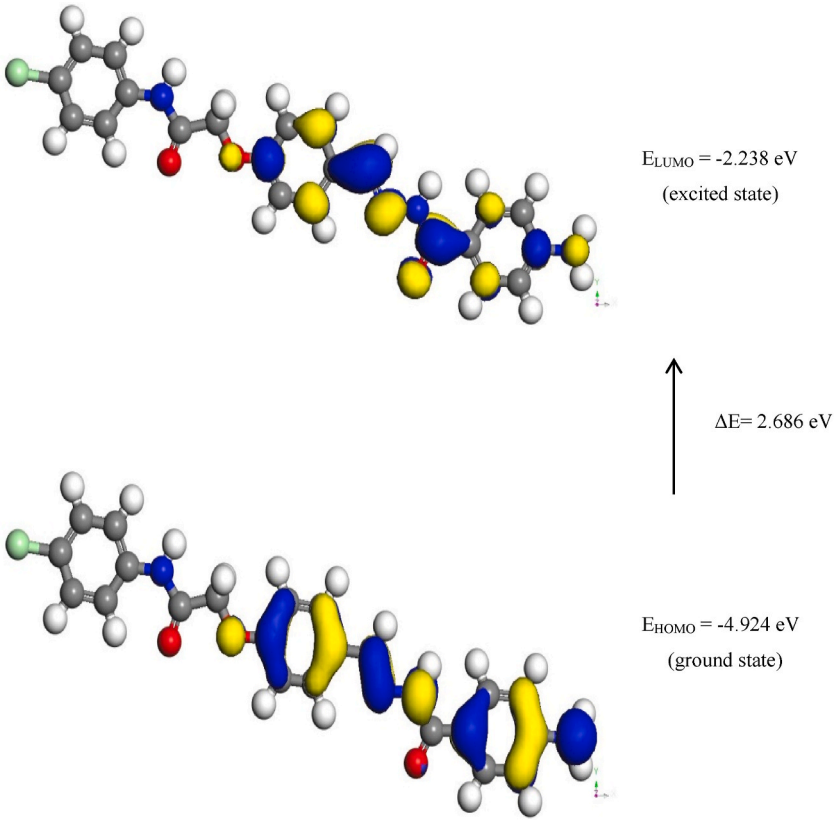

Fig. 5. Using the DFT approach, 3D plots of frontier orbital energies for **HL** (keto form).

Table 2
The **HL** and its complexes' estimated quantitative chemical properties.

Comp.	$-E_{HOMO}$ *(eV)*	$-E_{LUMO}$ *(eV)*	*ΔE (eV)*	*χ (eV)*	*η (eV)*	*σ (eV)* $^{-1}$	*–Pi (eV)*	*S (eV)* $^{-1}$	*ω (eV)*	ΔN_{max} *(eV)*
HL	4.924	2.238	2.686	3.581	1.343	0.745	3.581	0.372	4.774	2.666
(1)	4.450	2.337	2.113	3.394	1.057	0.947	3.394	0.473	5.450	3.212
(2)	4.471	2.392	2.079	3.432	1.040	0.962	3.432	0.481	5.664	3.301
(3)	4.177	2.428	1.749	3.303	0.875	1.144	3.303	0.572	6.236	3.776

1. The optimal location for metal ion is where HOMO level is localized, which is primarily on (C═N) groups in the free (Fig. 5).
2. In comparison to previous data discovered in free ligands, such as in N(20)–N(21) and C(22)–O(24), the coordination sites' bond lengths lengthened.
3. Because of development of a member of the double bond, bond lengths of coordination sites decreased in comparison to prior values seen in free ligands, such as in N(21)–C(22) [51].
4. The coordination of metals alters the bond angles of **HL** [52]. Angles between C(22)-N(21)-N(20), C(23)-C(22)-O(24), N(21)-C(22)-O(24), and N(20)-N(21)-C(22) that alter most when a complex forms as a result of bonding [53].
5. The Co(II), Ni(II), and Cu(II) complexes' bond angles resemble Oh geometry with sp^3d^2 hybrid orbitals quite a bit.
6. The weaker compounds that contribute electron capacity are indicated by lower HOMO energy levels. On additional side, the greater HOMO energy suggests that the molecule is an excellent electron donor. The LUMO energy is the potential of an electron-accepting molecule [54].

3.5.2. Chemical responsiveness

3.5.2.1. Descriptors of global reactivity. Fundamentally standard in quantum appreciations are the highest occupied molecular orbitals (HOMOs) and lowest unoccupied molecular orbitals (LUMOs), as well as orbitals in reference be border molecular orbitals (FMOs) (Fig. S4, Supplementary material). In order to calculate electron conductivity, which aids in explaining the molecular electrical transport features, the energy difference between the FMOs describes the stability of the molecule. (Eqs. (6)–(13)).

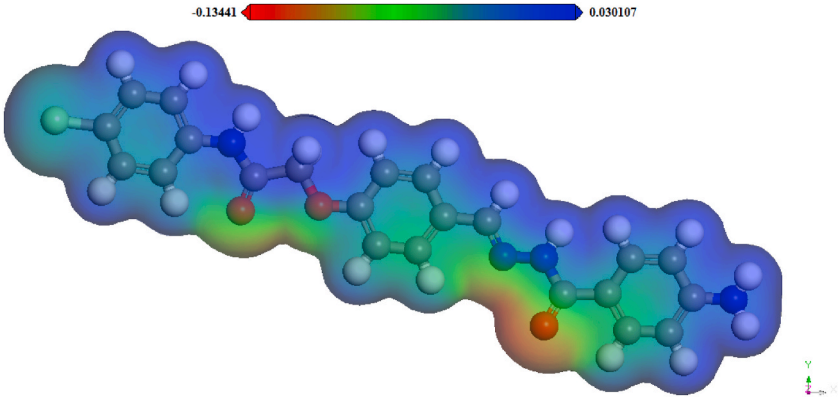

Fig. 6. Map of the molecular electrostatic potential for **HL**.

i. The fact that E_{HOMO} and E_{LUMO} are frequently practically negatives demonstrates how isolated compounds stabilize.
ii. The FMOs predicted that aromatic compounds' electrophilic attack sites would exist. These orbitals must be combined for a variety of responses.
iii. Using the Gutmann's variation principle, it was decided that E_{HOMO} would increase with lengthened M−L bonds and decrease in lengths of bonds next to the M-L sites [55].
iv. For the studied compounds, the chemical sensitivity and dynamical stability were described using the energy gap ($E = E_{HOMO}$-E_{LUMO}) [56].
vi. Both hardness and softness play significant roles in calculating reactivity and stability.
vii. Electrophilicity (ω), softness (S), hardness (η), potential (μ), electronegativity (χ), ΔE, E_{HOMO} and E_{LUMO} of **HL** and its chelates (**1**–**3**) [57,58] were presented in Table 2.

$$\Delta E = E_{LUMO} - E_{HOMO} \tag{6}$$

$$\chi = \frac{-(E_{HOMO} + E_{LUMO})}{2} \tag{7}$$

$$\eta = \frac{E_{LUMO} - E_{HOMO}}{2} \tag{8}$$

$$\sigma = 1/\eta \tag{9}$$

$$Pi = -\chi \tag{10}$$

$$S = \frac{1}{2\eta} \tag{11}$$

$$\omega = Pi^2/2\eta \tag{12}$$

$$\Delta N_{max} = -Pi/\eta \tag{13}$$

3.5.2.2. Molecular electrostatic potential. Surface electric potential plotted with same charge density is called the MEP [59]. By way of a 3D illustration, it is (Fig. 6). Red color symbolizes the favorable zone for electrophilic assaults, whereas blue color describes the favorable zone for nucleophilic attacks. Red, Green, and Blue are the colors in which the potential rises in intensity, with blue denoting the most powerful attraction also red denoting the most powerful repulsive. According to the MEP map, areas exhibiting positive potential are over the hydrogen atoms, and zones indicating negative potential are over the electronegative nitrogen atoms.

3.5.2.3. Mulliken population analysis. Atomic ions in a given molecule can be determined by computing its charge distribution. This affects the spectrum of vibrations, that in turn impact many other aspects of the system, such as the atoms' bond lengths, the dipole moment, the polarizability of molecules, their electronic structures, their acidity-basicity properties, and many more [60]. The related Mulliken's figure illustrates the DFT method for calculating Mulliken atomic charges (Fig. S5, Supplementary material). It is significant to remember of the **HL** atoms that have a positive charge and have become more acidic are C(1), C(2), C(5), C(8), C(13), C(16), C(19), C(22), C(27), and H(31), while the atoms that have a negative charge are O(3), N(4), C(6), C(7), N(4), C(6), C(7), N(4), C(6), C(7), N (4), C(6), C(7)), C(9), C(10), C(11), C(12), C(14), C(15),C(17), C(18), N(20), N(21), C(23), C(24), C(25), C(26), C(28), C(29) and N(30) atoms. The maximum atomic charge for an O(24) atom is around −0.572, while the C(22) atom in the $(C{=}N)_{azomethine}$ group has the highest possible positive atomic charge.

Table 3
DMOL^3 computed certain energy characteristics of **HL** and its complexes (**1–3**) using the DFT method.

Compound	Energy components (kcal/mol)							Dipole moment (D)
	Total of the atomic energies	Kinetic energy	Electrostatic energy	Exchang-Corelation energy	Energy from spin polarisation	Overall Energy	Binding Energy	
HL	−1095719.6	−8471.3797	−1245.3199	2290.9058	1757.86212	−1101389.36	−5668.22	14.9297
(1)	−1438232.4	−8061.6076	−3997.16334	2880.53818	2169.98721	−1445233.37	−7008.25	9.5543
(2)	−1454970.9	−7818.9569	−4193.05773	2873.59723	2140.159106	−1461962.10	−6998.26	9.0296
(3)	−1473222.4	−9718.7384	−2105.27390	2796.342138	2118.398579	−1480121.81	−6909.27	10.3193

Table 4
Data about the ligand's (**HL**) thermal analyses and its complexes (**1**–**3**).

Compound	Step	Temperature range (°C)	mass loss (calc.)%	Identification
HL	1St	170–420	50.66 (50.67)	Loss of $C_{12}H_{12}ON_3$
	2nd	418–650	46.50 (46.49)	Loss of $C_9H_7ClO_2N$
	Residue	630–750	2.84 (2.84)	Residue: C atom
(1)	1St	70–120	2.98 (3.03)	Loss of H_2O (solv.)
	2nd	120–353	37.12 (37.08)	Loss of $2H_2O$(coord.)+CH_3COO + $C_6H_9ON_2$
	3rd	353–575	26.27 (45.25)	Loss of $C_{15}H_9ClN_2O$
	Residue	575–750	14.63 (14.64)	Residue: C atom + CoO
(2)	1St	70–97	3.02 (3.03)	Loss of H_2O (solv.)
	2nd	145–345	37.07 (37.10)	Loss of $2H_2O$(coord.)+CH_3COO + $C_6H_9ON_2$
	3rd	345–524	47.32 (47.29)	Loss of $C_{16}H_9ClN_2O$
	Residue	524–750	12.59 (12.58)	Residue: NiO
(3)	1St	70–269	18.88 (18.89)	Loss of H_2O (solv.)+$2H_2O$(coord.)+CH_3COO
	2nd	269–579	65.82 (65.81)	Loss of $C_{21}H_{18}ClO_2N_4$
	Residue	579–750	15.30 (15.30)	Residue: C + CuO

Table 5
Kinetic characteristics of the ligand (**HL**) and its chelates (**1–3**).

Comp.	Temp. (°C)	Method	Parameters					R^2
			Ea (kJ.mol^{-1})	A (s^{-1})	− ΔS* (J.mol^{-1}K^{-1})	ΔH* (kJ.mol^{-1})	ΔG* (kJ.mol^{-1})	
HL	First step	CR	99.69	1.59 10^6 ×	131.74	94.85	171.54	0.99974
		HM	110.06	1.30 ^{7}10 ×	114.84	104.89	176.36	0.99945
	Second step	CR	100.71	9.09 ^{3}10 ×	177.41	94.00	237.03	0.98718
		HM	114.29	6.91 ^{4}10 ×	160.94	107.26	243.33	0.99605
(1)	First step	CR	76.07	2.08 ^{9}10 ×	68.19	73.04	97.87	0.97178
		HM	82.00	1.58 10^{10} ×	51.31	78.98	97.66	0.97156
	Second step	CR	92.36	2.77 ^{7}10 ×	106.59	88.27	140.69	0.97683
		HM	100.37	2.11 × 10^8	89.72	96.27	140.43	0.9754
	Third step	CR	99.07	1.81 ^{4}10 ×	170.98	92.91	219.57	0.99899
		HM	111.60	1.53 ^{5}10 ×	153.24	105.44	218.96	0.99827
(2)	First step	CR	69.55	3.48 10^8 ×	82.63	66.68	95.25	0.97289
		HM	75.55	2.83 10^9 ×	65.47	72.58	95.93	0.9719
	Second step	CR	96.62	4.98 ^{7}10 ×	101.91	92.44	143.65	0.98541
		HM	104.84	3.83 × 10^8	84.93	100.66	143.34	0.98411
	Third step	CR	95.62	3.90 ^{4}10 ×	164.09	89.81	204.33	0.95618
		HM	106.51	2.81^{5}10 ×	147.65	100.72	203.57	0.95628
(3)	First step	CR	97.57	9.26 × 10^7	96.95	93.28	143.22	0.99267
		HM	106.28	7.68 × 10^8	79.35	102.00	142.87	0.99563
	Second step	CR	78.49	2.68 × 10^4	165.91	73.53	172.42	0.99888
		HM	88.74	2.37 × 10^5	147.81	83.77	172.08	0.99713

3.5.2.4. Dipole energy and other atomic characteristics. The binding energy measurements demonstrated which products are more stable than ligand [61]. We observed a rise in the complexes' computed binding energy values when compared to the ligand's values. Additionally, the DFT process was used to determine the energy of various materials (Table 3).

3.6. TGA studies

Thermal evaluation (TGA) was employed to get significant data about the thermal stability of the synthesized compounds (**HL**) and its chelates (**1–3**) and to inspect the nature of solvent molecules (if existing) to be outside or inside the metal's internal coordinating sphere [62–64]. (Fig. S6, Supplementary material). Table 4 includes the stages of degradation, range of temperature, and degradation products, and weight loss % of certain metal complexes. The outcomes agreed with the findings of a simple analysis. The chelates

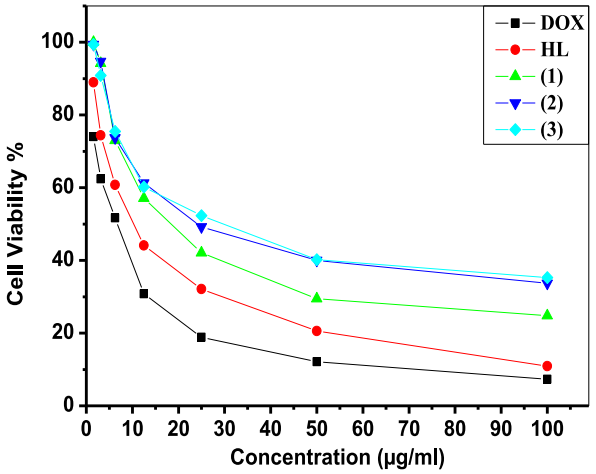

Fig. 7. Comparing survival of **HELA** cells cultured for 24 h at various **HL** and its complexes concentrations (**1**–**3**).

showed different stages of the disintegration process after reaching the dehydration stage. The ultimate mass loss results from meltdown of leftover carbon atoms and lingering metal oxide [62].

The thermal decomposition of the hydrazone ligand takes place at higher temperatures comparative to its complexes. This may be attributed to the presence of intramolecular H-bonding in the hydrazone ligand [65–67].

From either the TG and DTG, the order (n) and activation energy Ea of the several breakdown phases were estimated via Coats-Redfern [68] also Horowitz-Metzger [69] methods to be able to evaluate effects of the structural characteristics of ligand and title metal on thermal behaviour of chelates (Figs. S7 and S8, Supplementary material) E_a, A, ΔS^*, ΔH^* and ΔG. In example, Table 5 has suggested a first order for the breakdown of ligands (HL) and their complexes (**1–3**).

The Arrhenius equation's expression for ratio of thermal breakdown of a compound $\frac{d\alpha}{dt}$ takes following form (Eq. 14).

$$\frac{d\alpha}{dt} = A\exp\left(-\frac{Ea}{RT}\right)g(\alpha) \tag{14}$$

in where n indicates the reaction order, which is thought to remain unchanged during the reaction, and Ea is the activation energy where A is the Arrhenius preexponential factor, R is the gas constant, and g(α) is the differential conversion factor and equals $(1 - \alpha)^n$.

Numerous breakdown processes, including the investigation's succession of metal complexes degrading, can be modeled as first order reactions [70]. In light of this supposition, the integration of Eq. (15) results in:

$$\ln(1-\alpha) = -\frac{A}{\beta}\int_{T_0}^{T} Exp\left(-\frac{E_a}{RT}\right)dT \tag{15}$$

It is possible to use the integral approach to examine experimental data and determine the kinetic models for deterioration A, Ea. The Eyring equation can be used to compute the additional thermodynamic characteristics of activation [71,72]. Based on the findings, the following observations are made:

i. For all decomposing steps, n = 1 exhibits the best fit.
ii. Due to the covalent nature of these chelates, the complexes' high Ea values demonstrate their remarkable constancy [73]. Ea values are **HL** > Cu(II) > Ni(II) > Co(II) complex, in that sequence. As a result, in this order, the thermal stability rises.

The following thermodynamic activation parameters can be derived using the Eyring equations (Eqs. (16)–(18)):

$$\Delta H^* = E_a - RT \tag{16}$$

$$\Delta S^* = 2.303\left[\log\left(\frac{Ah}{K_B T_S}\right)\right]R \tag{17}$$

$$\Delta G^* = \Delta H^* - T\Delta S^* \tag{18}$$

A complex does not spontaneously dissolve, as evidenced by the positively significant of G. The negative numbers of ΔS* are related to low stored energy. The positive measurement of ΔH* indicates that the thermal decomposition is an endothermic reaction.

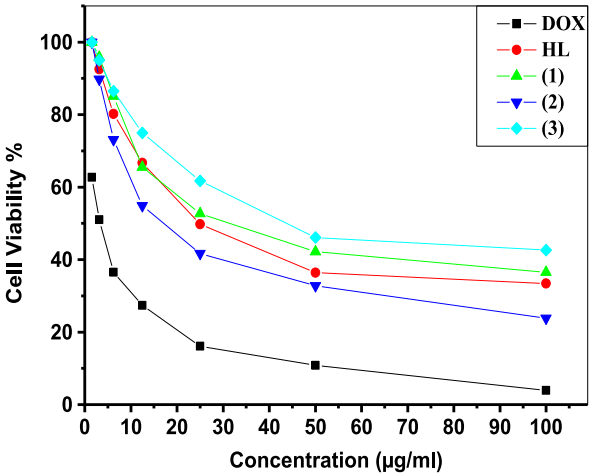

Fig. 8. Comparing vitality of WISH cells treated for 24 h at various **HL** and its complexes (**1**–**3**) concentrations.

Table 6
Human cell line-specific cytotoxicity of **HL** and its complexes (**1–3**) the **WISH** and **Hela** cell lines.

Compound	Hela	WISH
DOX	5.57 ± 0.4	3.18 ± 0.2
HL	10.14 ± 0.7	25.90 ± 0.6
(1)	19.67 ± 2.0	31.01 ± 2.9
(2)	24.21 ± 2.2	18.28 ± 1.8
(3)	31.43 ± 2.6	43.34 ± 3.8

• IC_{50} (μM): 1–10 (very powerful). 11–20 (strong). 21–50 (moderate). 51–100 (weak) and more than 100 (non-cytotoxic), Doxorubicin (DOX).

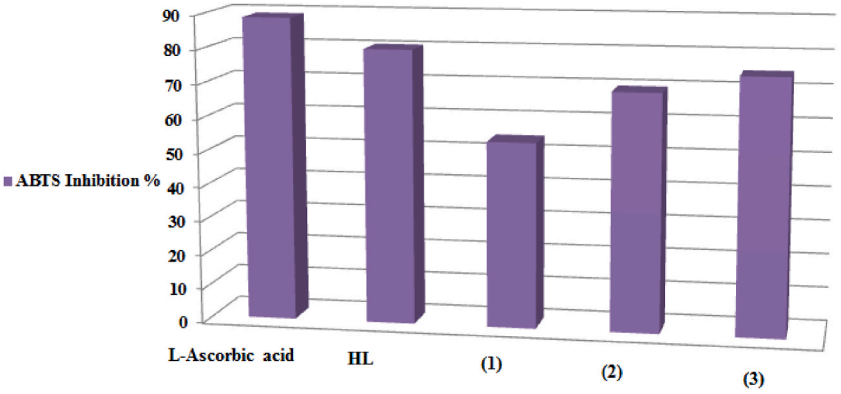

Fig. 9. ABTS Inhibition % of **HL** and its chelates (**1**–**3**).

Table 7
ABTS Inhibition **%** of **HL** and its metal complexes (**1–3**).

ABTS assay	
Compounds	*ABTS* Inhibition %
L-Ascorbic acid	88.8
HL	80.2
(1)	54.3
(2)	69.5
(3)	74.7

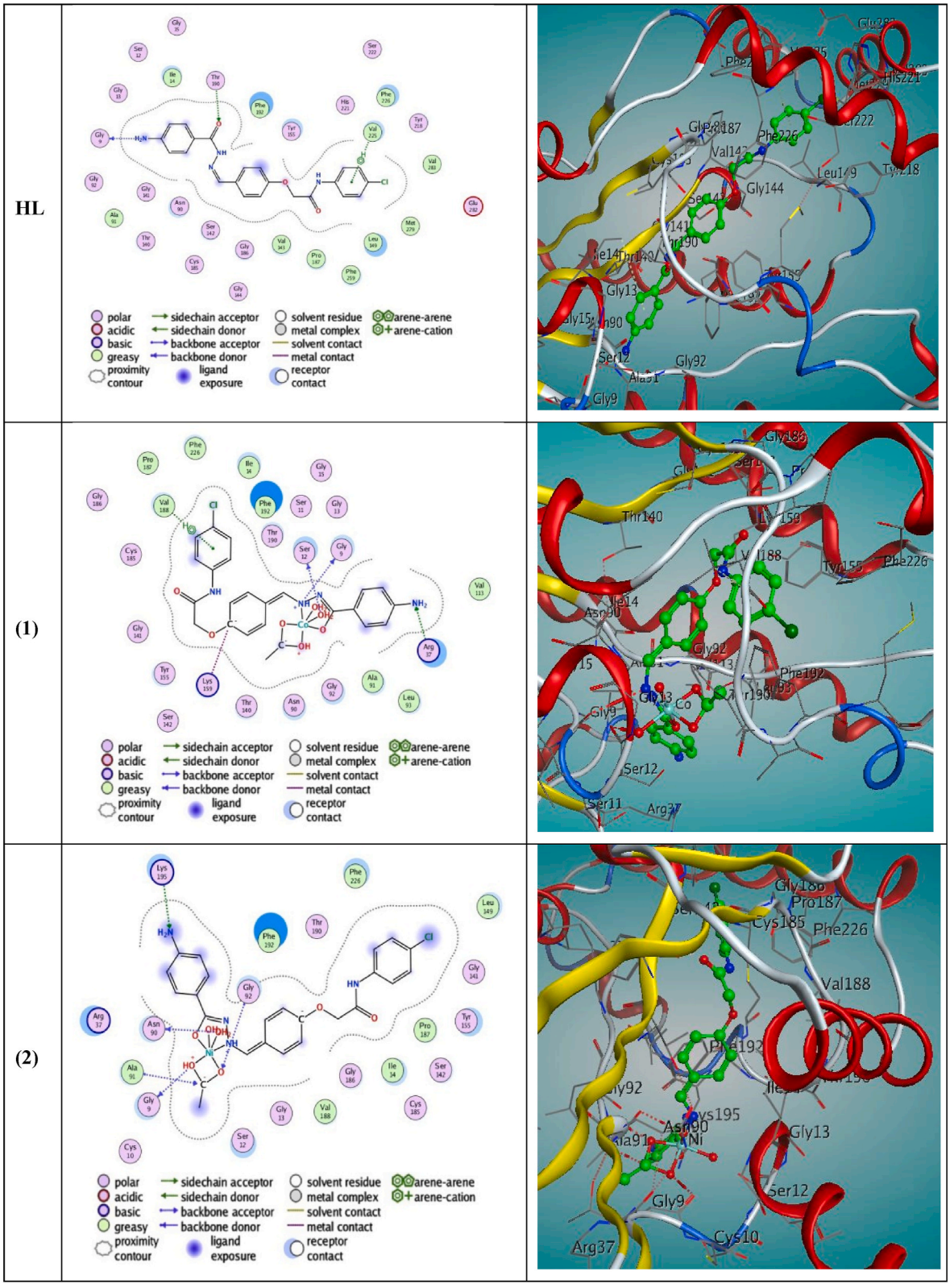

Fig. 10. Interaction diagrams in two- and three-dimensions of **HL** and its complexes (**1–3**) with breast cancer gene 3hb5.

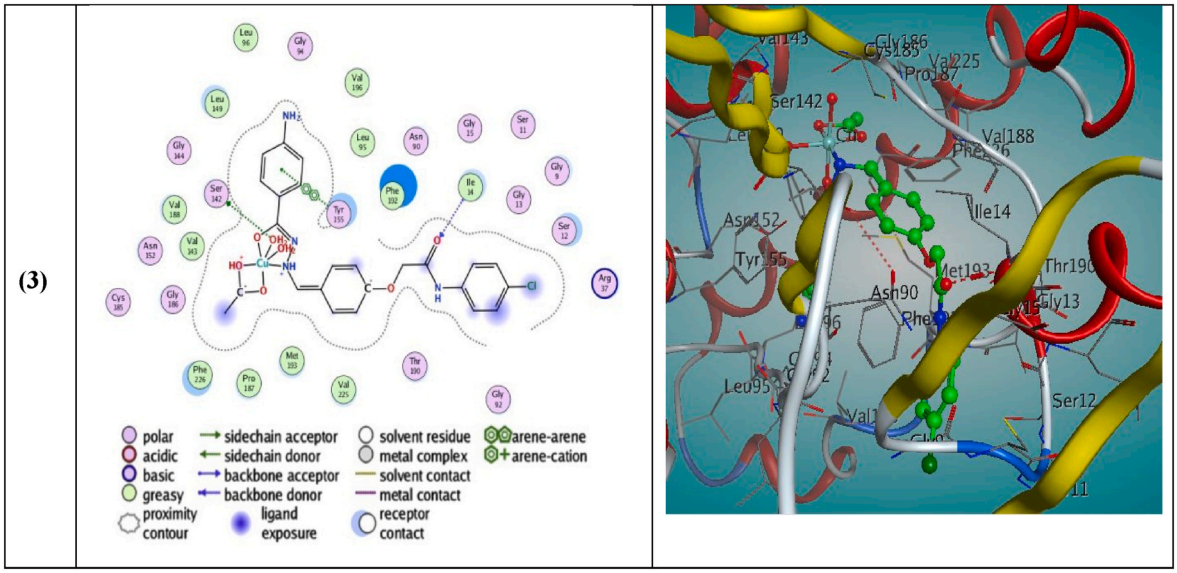

Fig. 10. (*continued*).

3.7. Biological function

3.7.1. Antitumor function

Utilizing doxorubicin (DOX) as a reference compound, Antitumor function of ligand also its chelates (**1–3**) is assessed for invitro anticancer effective towards both epitheliod carcinoma (**Hela**) and human amnion (**WISH**) (referring to Figs. 7 and 8) [74,75]. As a reference medication, using doxorubicin (DOX), among the most powerful cancer treatments. IC_{50}, or the amount of a material (in μg/mL) blocks tumour cell's ability to proliferate in 50% relative to the baseline, unexamined cells is how the activity data are expressed [76]. The estimated IC_{50} values are shown in Table 6, and they show that the studied drugs, **HL** and The Co(II) chelates (**1**), have great cytotoxic effect towards **Hela** cellular lines give IC_{50} values of 10.14±0.7 and 19.67±2.0 μg/mL, respectively. While Ni(II) and Cu(II) complexes exhibit a moderate level of cytotoxicity against **Hela** cellular lines, respective IC_{50} is 24.21±2.2 and 31.43±2.6 μg/mL. Regarding **WISH (HL)** ligand, Co(II), and Cu(II) chelates show moderate antitumor function towards **WISH** cellular lines give IC_{50} = 25.90±0.6, IC_{50} = 31.01±2.9 and 43.34±3.8 μg/mL, respectively, when matched to doxorubicin. The Ni(II) complex (**2**) only exhibited a strong effective anticancer on **WISH** cell cultures IC_{50} = 18.28±1.8 (Fig. 9, Supplementary material).

3.7.2. Antioxidant activity using ABTS inhibition

Using the ABTS technique, the Schiff base and its complexes too were tested for its capacity to scavenge free radicals [77]. Fig. 9 displays the study materials' free radical scavenging activity maximum inhibition findings. Analyzing the information in Table 7 reveals that every chemical demonstrates strong anti-oxidative action. **HL** > Cu(II) complex > Ni(II) complex > Co(II) complex is a possible order for the chemicals [78].

3.8. Molecular docking study

One of the most crucial techniques for predicting possibility for restriction and interaction manner also mechanical details of biochemical moiety in enzyme's sector is molecular docking modeling [79,80]. To predict the connections between synthetic chemicals and enzyme targets, one can use a trustworthy computational method. Additionally, it is used to look into the molecule's optimum orientations and binding characteristics that lead to a novel chelates with zero or very little energy.

In this investigation, we used the Molecular Operating Environment (MOE, 2015.10) tool to connect the ligand **HL** and its chelates (**1–3**) to breast cancer mutant (PDB ID 3hb5) and Crystal Structure identified in Cervical Cancer (PDB ID 4J96). The findings showed that substances and receptor proteins might be combined. They were examined for their docking conformations with various protein receptors in considerations of hydrogen bonding, binding energy, and hydrophobic interactions [81,82].

Additionally, shown in the two - dimensional and three - dimensional plots were interconnections between produced compounds and various receptors (Figs. 10 and 11). With the amino acids GLY, THR, and VAL, the ligand displayed three interactions. These interconnections were H—donor, H—acceptors also pi—H links, that ligand displayed the least amount of binding energy −7.7972 and − 7.0125 kcal/mol for 3hb5 and 4J96, and minor RMSD of 1.6808 Å between the co-crystallized drug and the interaction position [83, 84], if experimental conformation's RMSD from the native ligand's best docked conformation is ≤ 2.0 Å, By successfully replicating all of the important contacts made via the ligand that is co-crystallized with key amino acids (hot spots) in the active, as well as by the success of the scoring function that is being employed.

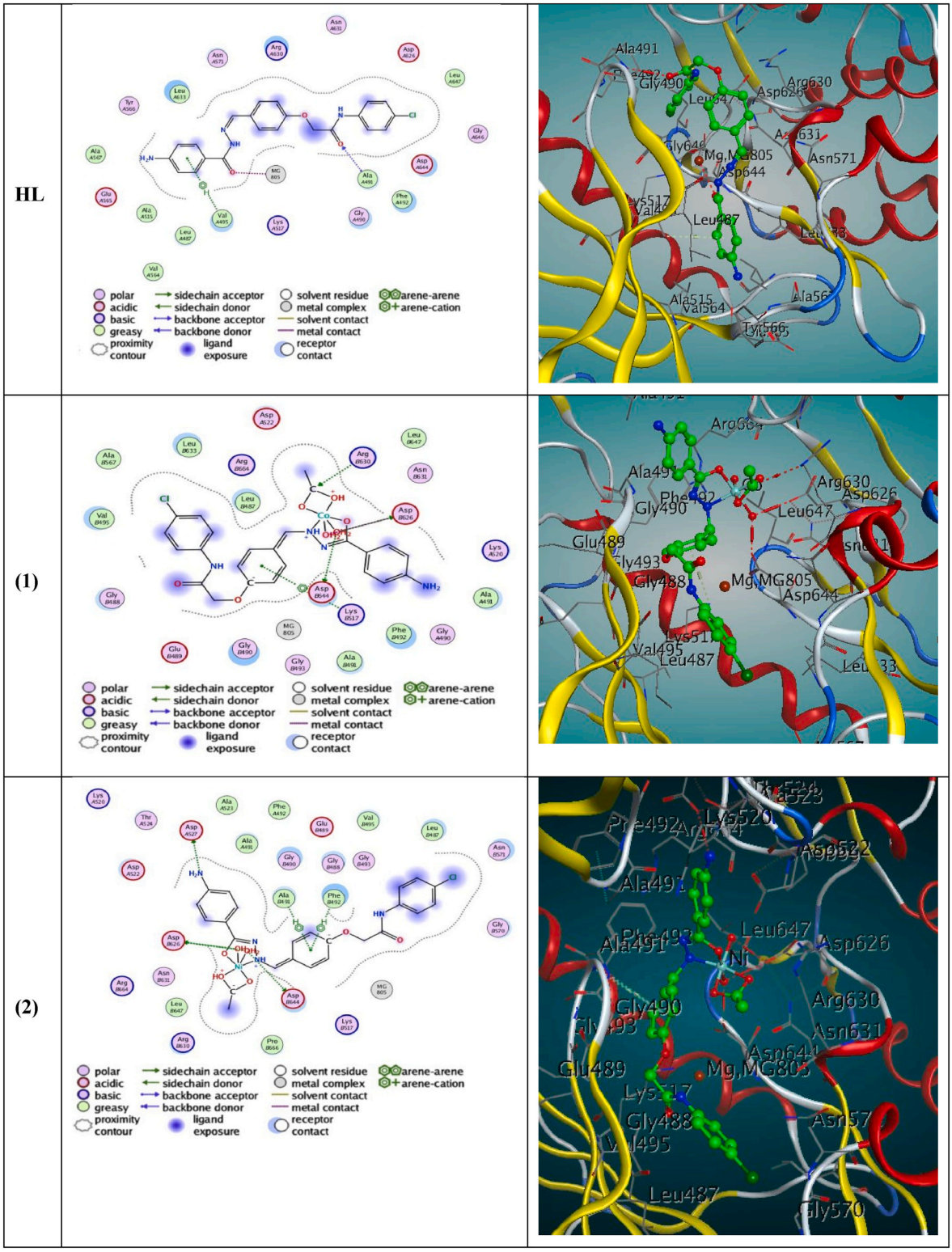

Fig. 11. Interaction diagrams in two- and three-dimensions of **HL** and its complexes (**1–3**) with Crystal Structure identified in Cervical Cancer (PDB ID 4J96).

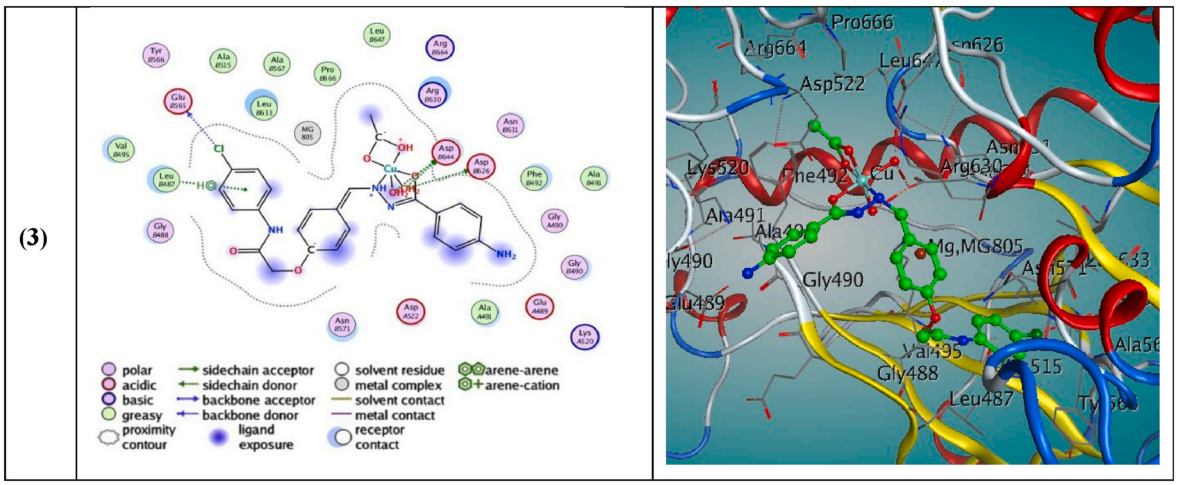

Fig. 11. (*continued*).

While Co(II), Ni(II), and Cu(II) complexes demonstrated additional interactions such as H-donor, pi-H, and ionic links in addition to H-acceptors and pi-cation. Also binding energies for the Co(II), Ni(II), and Cu(II) complexes, respectively, existed be −7.0275, −6.0430, and −6.3628 for 3hb5 and -6.9120, −6.7243 and −6.6571 for 4J96 were determined via studies of computerized docking. Table S9 (Supplementary material) provides the energy values, the present compounds have a binding free energy is negative, which points to a strong protein binding [85]. In comparison to the ligand and other complexes, complex (**2**)'s more negative relative binding energy shows a greater ability to link to protein.

4. Conclusion

This work defines production, description procedures, and anticancer activity of hydrazone (**HL**) and its Co(II), Ni(II), and Cu(II) chelates (**1–3**). The metal chelates are octahedral structure with the ligand (**HL**) acting as a monobasic bidentate coordinating via the oxygen atom of (−C═O) group in enol form and N atom of the $(-C{=}N-)_{azomethine}$ group, according to UV, thermal, and theoretic information. Thermal analysis (TGA and DrTGA) and the negative values of the energies of HOMO and LUMO both indicate compounds are stable. Utilizing doxorubicin (DOX) as a reference compound, Antitumor function of ligand also its chelates (**1–3**) is assessed for invitro anticancer effective towards both epitheliod carcinoma (HeLa) and human amnion (WISH). These results observed that **HL** and The Co(II) chelates (**1**), have great cytotoxic effect towards **Hela** cellular lines give IC_{50} values of 10.14±0.7 and 19.67 ±2.0 μg/mL, respectively. To indicate the effect of **HL** and its complexes against breast cancer mutants by interacting with receptor Protein (PDB ID 3hb5), molecular docking was used by (MOE, 2015.10) program. In additional hand, the prepared compounds are helpful in the applications for therapy.

Author contribution statement

Fatmah Alkhatib: Analyzed and interpreted the data; Contributed reagents, materials, analysis tools or data; Wrote the paper.
Hajar Mubashir Alsulami: Conceived and designed the experiments; Performed the experiments; Analyzed and interpreted the data.

Data availability statement

Data will be available on request.

Declaration of competing interest

The authors declare that they have no known competing financial interests or personal relationships that could have appeared to influence the work reported in this paper.

Appendix A. Supplementary data

Supplementary data to this article can be found online at https://doi.org/10.1016/j.heliyon.2023.e18988.

References

[1] A. Singh, S. Kr Maiti, H.P. Gogoi, P. Barman, Purine-based Schiff base Co(II), Cu(II), and Zn(II) complexes: synthesis, characterization, DFT calculations, DNA binding study, and molecular docking, Polyhedron 230 (15) (2023), 116244.
[2] A.A. Abdel Aziz, R.M. Ramadan, M.E. Sidqi, M.A. Sayed, Structural characterisation of novel mononuclear Schiff base metal complexes, DFT calculations, molecular docking studies, free radical scavenging, DNA binding evaluation and cytotoxic activity, Appl. Organomet. Chem. 37 (2) (2023), e6954.
[3] M. Dolai, U. Saha, A simple Cu(II) complex of phenolic oxime: synthesis, crystal structure, supramolecular interactions, DFT calculation and catecholase activity study, Heliyon 6 (10) (2020), e04942.
[4] F. Samy, M. Shebl, Co(II), Ni(II), and Cu(II) complexes of 4,6-bis(2-hydroxynaphthalen-1-yl)methyl-ene)hydrazono)ethyl)benzene-1,3-diol: synthesis, spectroscopic, biological, and theoretical studies, Appl. Organomet. Chem. 36 (5) (2022), e6650.
[5] S. Kumar, J. Devi, A. Dubey, D. Kumar, D.K. Jindal, S. Asija, A. Sharma, Co(II), Ni(II), Cu(II) and Zn(II) complexes of Schiff base ligands: synthesis, characterization, DFT, in vitro antimicrobial activity and molecular docking studies, Res. Chem. Intermed. 49 (2023) 939–965.
[6] S. Gemma, G. Kukreja, C. Fattorusso, M. Persico, M.P. Romano, M. Altarelli, L. Savini, G. Campiani, E. Fattorusso, N. Basilico, D. Taramelli, V. Yardley, S. Butini, Synthesis of N1-arylidene-N2-quinolyl- and N2-acrydinylhydrazones as potent antimalarial agents active against CQ-resistant P. falciparum strains, Bioorg. Med. Chem. Lett. 16 (2006) 5384–5388.
[7] A.L. Berhanu, I. Mohiuddin, A.K. Malik, J.S. Aulakh, V. Kumar, K.H. Kim, A review of the applications of Schiff bases as optical chemical sensors, Trends Anal. Chem. 116 (2019) 74–91.
[8] K. Pyta, A. Janas, M. Szukowska, P. Pecyna, M. Jaworska, M. Gajecka, F. Bartl, P. Przybylski, Synthesis, docking and antibacterial studies of more potent amine and hydrazone rifamycin congeners than rifampicin, Eur. J. Med. Chem. 167 (2019) 96–104.
[9] N.R. Palepu, J.R. Premkumar, A.K. Verma, K. Bhattacharjee, S.R. Joshi, S. Forbes, Y. Mozharivskyj, K.M. Rao, Antibacterial, in vitro antitumor activity and structural studies of rhodium and iridium complexes featuring the two positional isomers of pyridine carbaldehyde picolinic hydrazone ligand Production and hosting by Elsevier, Arab. J. Chem. 11 (2018) 714–728.
[10] A. Erguc, M.D. Altintop, O. Atli, B. Sever, G. Iscan, G. Gormus, A. Ozdemir, Synthesis and biological evaluation of new quinoline-based thiazolyl hydrazone derivatives as potent antifungal and anticancer agents, Lett. Drug Des. Discov. 15 (2018) 193–202.
[11] C.-G. Li, H.-L. An, L.-Q. Chai, Synthesis, spectroscopic studies, and single-crystal structures of two 3-D supramolecular zinc (II) and nickel (II) complexes containing thiazole ring: antimicrobial assays, time-dependent density functional theory calculations, and Hirshfeld surface analysis, Appl. Organomet. Chem. 37 (1) (2023), e6918.
[12] A. Savcı, K. Buldurun, G. Kırkpantur, A new Schiff base containing 5-FU and its metal Complexes: synthesis, Characterization, and biological activities, Inorg. Chem. Commun. 134 (2021), 109060.
[13] A. Savcı, K. Buldurun, M.E. Alkış, Y. Alan, N. Turan, Synthesis, characterization, antioxidant and anticancer activities of a new Schiff base and its M(II) complexes derived from 5-fluorouracil, Med. Oncol. 39 (11) (2022) 1–11.
[14] M. Shebl, M. Saif, A.I. Nabeel, R. Shokry, New non-toxic transition metal nanocomplexes and Zn complex-silica xerogel nanohybrid: synthesis, spectral studies, antibacterial, and antitumor activities, J. Mol. Struct. 1118 (2016) 335–343.
[15] R.-S. Mezey, I. Máthé, S. Shova, M.-N. Grecu, T. Roşu, Synthesis, characterization and antimicrobial activity of copper (II) complexes with hydrazone derived from 3-hydroxy-5-(hydroxymethyl)-2-methylpyridine-4-carbaldehyde, Polyhedron 102 (2015) 684–692.
[16] S. Mondal, C. Das, B. Ghosh, B. Pakhira, A.J. Blake, M.G.B. Drew, S. Kumar Chattopadhyay, Synthesis, spectroscopic studies, X-ray crystal structures, electrochemical properties and DFT calculations of three Ni(II) complexes of aroyl hydrazone ligands bearing anthracene moiety, Polyhedron 80 (2014) 272–281.
[17] A.A. Khandar, N.N. Ramazani, S.S. Balula, B. Shaabani, L. Cunha-Silva, H. Mobaiyen, Novel pseudohalide-bridged Cu(II) complexes with a hydrazone ligand: evaluation of antimicrobial activity, Polyhedron 80 (2014) 166–172.
[18] Ö. Özge, D. Avcı, F. Sönmez, Ö. Tamer, N. Dege, A. Başoğlu, Y. Atalay, B.Z. Kurt, Synthesis, DFT calculations, α-glucosidase inhibitor activity, and docking studies on Schiff base metal complexes containing isothiocyanate, Appl. Organomet. Chem. 37 (5) (2023), e7084.
[19] Y. Deswal, S. Asija, A. Tufail, A. Dubey, L. Deswal, N. Kumar, S. Saroya, J.S. Kirar, N.M. Gupta, Instigating the in vitro antidiabetic activity of new tridentate Schiff base ligand appended M(II) complexes: from synthesis, structural characterization, quantum computational calculations to molecular docking, and molecular dynamics simulation studies, Appl. Organomet. Chem. 37 (4) (2023), e7050.
[20] K. Buldurun, N. Turan, E. Bursal, A. Aras, A. Mantarcı, N. Çolak, F. Türkan, İ. Gülçin, Determination of anticancer properties and inhibitory effects of some metabolic enzymes including acetylcholinesterase, butyryl cholinesterase, alpha-glycosidase of some compounds with molecular docking study, J. Biomol. Struct. Dynam. 39 (17) (2021) 6480–6487.
[21] A.M. Abu-Dief, N.M. El-Metwaly, S.O. Alzahrani, F. Alkhatib, M.M. Abualnaja, T. El-Dabea, M.A.A. El-Remaily, Synthesis and characterization of Fe(III), Pd(II) and Cu(II)-thiazole complexes; DFT, pharmacophore modeling, in-vitro assay and DNA binding studies, J. Mol. Liq. 326 (2021), 115277.
[22] H. Katouah, A.M. Hameed, A. Alharbi, F. Alkhatib, R. Shah, S. Alzahrani, R. Zaky, N.M. El-Metwaly, Green synthesis strategy for new Schiff-Base complexes: characterization, conductometry, in vitro assay confirmed by in silico approach, ChemistrySelect 5 (2020) 10256–10268.
[23] Y.M. Ahmed, A.M. Ashmawy, A.A. Abbas, G.G. Mohamed, Synthesis, characterization, antibacterial, antioxidant activities, density functional theory, and molecular docking studies of new organic metal complexes and links to application of corrosion inhibitors, Appl. Organomet. Chem. 37 (4) (2023), e7015.
[24] X. Wu, A.K. Ray, Interference between extrinsic and intrinsic losses in x-ray absorption fine structure, Phys. Rev. B 65 (2002) 85403–85409.
[25] W.J. Hehre, L. Radom, P.V.R. Schleyer, J.A. Pople, Ab Initio Molecular Orbital Theory, John Wiley, New York, 1986.
[26] Materials Studio, Accelrys software Inc., San Diego, USA, 2011.
[27] B. Hammer, L.B. Hansen, J.K. Nørskov, Improved adsorption energetics within density-functional theory using revised Perdew-Burke-Ernzerhof functionals, Phys. Rev. B 59 (1999) 7413.
[28] A. Matveev, M. Staufer, M. Mayer, N. Rösch, Density functional study of small molecules and transition-metal carbonyls using revised PBE functionals, Int. J. Quant. Chem. 75 (1999) 863–873.
[29] T.A. Halgren, Parameterization, and performance of MMFF94, J. Comput. Chem. 17 (1996) 490–519.
[30] https://www.rcsb.org/.
[31] T. Mosmann, Rapid colorimetric assay for cellular growth and survival: application to proliferation and cytotoxicity assays, J. Immunol. Methods 65 (1983) 55–63.
[32] R.G. Deghadi, A.E. Elsharkawy, A.M. Ashmawy, G.G. Mohamed, Antibacterial and anticorrosion behavior of bioactive complexes of selected transition metal ions with new 2-acetylpyridine Schiff base, Appl. Organomet. Chem. 36 (4) (2022), e6579.
[33] N. Pellegrini, M. Ying, C. Rice-Evans, Screening of dietary carotenoids and carotenoid-rich fruit extracts for antioxidant activities applying 2,2'-azinobis (3-ethylenebenzothiazoline-6-sulfonic acid) radical cation decolorization assay, Methods Enzymol. 299 (1999) 379–384.
[34] A.F. Shoair, A.A. El-Bindary, M.K. Abd El-Kader, Structural and catalytic properties of some azo-rhodanine Ruthenium (III) complexes, J. Mol. Struct. 1143 (2017) 100–115.
[35] O.A. El-Gammal, F.Sh Mohamed, G.N. Rezk, A.A. El-Bindary, Synthesis, characterization, catalytic, DNA binding and antibacterial activities of Co(II), Ni(II) and Cu(II) complexes with new Schiff base ligand, J. Mol. Liq. 326 (2021), 115223.
[36] M.S. El-Attar, F.M. Ahmed, S.A. Sadeek, S.F. Mohamed, W.A. Zordok, W.H. El-Shwiniy, Characterization, DFT, and antimicrobial evaluation of some new N2O2 tetradentate Schiff base metal complexes, Appl. Organomet. Chem. 36 (10) (2022), e6826.
[37] O.M.I. Adly, M. Shebl, E.M. Abdelrhman, B.A. El-Shetary, Structural variety of Cu(II), Ni(II) and Co(II) complexes of a hydrazone based on 5-acetyl-4-hydroxy-2H-1,3-thiazine-2,6(3H)-dione: synthesis, spectroscopic, DFT, antitumor and docking studies, Appl. Organomet. Chem. 37 (4) (2023), e7036.
[38] H. Kabeer, S. Hanif, A. Arsalan, S. Asmat, H. Younus, M. Shakir, Structural-dependent N,O-donor imine-appended Cu(II)/Zn(II) complexes: synthesis, spectral, and in vitro pharmacological assessment, ACS Omega 5 (2020) 1229–1245.

[39] D.K. Rastogi, S.K. Sahni, V.B. Rana, S.K. Dua, Dimeric tetrahedral complexes of manganese (II) and iron (II) with benzoyl hydrazones, Trans. Met. Chem. 3 (1978) 56–60.
[40] A. Bartyzel, Synthesis, thermal study and some properties of N_2O_4 donor Schiff base and its Mn(III), Co(II), Ni(II), Cu(II) and Zn(II) complexes, J. Therm. Anal. Calorim. 127 (2017) 2133–2147.
[41] W.T. Carnall, S. Siegel, J.R. Ferraro, B. Tani, E. Gebert, New series of anhydrous double nitrate salts of the lanthanides. Structural and spectral characterization, Inorg. Chem. 12 (1973) 560.
[42] F. Samy, F.M. Omar, Synthesis, characterization, antitumor activity, molecular modeling and docking of new ligand,(2, 5-pyrrole)-bis (5, 6-diphenyl-[1, 2, 4]-triazin-3-yl) hydrazone and its complexes, J. Mol. Struct. 1222 (2020), 128910.
[43] D.X. West, Y. Yang, T.L. Klein, K.I. Goldberg, A.E. Liberta, J. Valdes Martinez, S. Hernandez-Ortega, Dinuclear nickel (II) complexes of 2-hydroxyacetophenone ^{4}N-substituted thiosemicarbazones, Polyhedron 14 (1995) 3051–3060.
[44] O.A. El-Gammal, H. Alshater, H.A. El-Boraey, Schiff base metal complexes of 4-methyl-1H-indol-3-carbaldehyde derivative as a series of potential antioxidants and antimicrobial: synthesis, spectroscopic characterization and 3D molecular modeling, J. Mol. Struct. 1195 (2019) 220–230.
[45] N. Nakamoto, Infrared Spectra and Raman Spectra of Inorganic and Coordination Compounds, fifth ed., Wiley, New York, 1997.
[46] A.A. El-Bindary, S.M. El-Marsafy, A.A. El-Maddah, Enhancement of the photocatalytic activity of ZnO nanoparticles by silver doping for the degradation of AY99 contaminants, J. Mol. Struct. 1191 (2019) 76–84.
[47] V.S. Bystrov, C. Piccirillo, D.M. Tobaldi, P.M.L. Castro, J. Coutinho, S. Kopyl, R.C. Pullar, Oxygen vacancies, the optical band gap (Eg) and photocatalysis of hydroxyapatite: comparing modelling with measured data, Appl. Catal. B Environ. 196 (2016) 100–107.
[48] A. Slepko, A.A. Demkov, First-principles study of the biomineral hydroxyapatite, Phys. Rev. B 84 (2011), 134108.
[49] M.E. Awad, A.M. Farrag, A.A. El-Bindary, M.A. El-Bindary, H.A. Kiwaan, Photocatalytic degradation of Rhodamine B dye using lowcost pyrofabricated titanium dioxide quantum dotskaolinite nanocomposite, Appl. Organomet. Chem. 37 (7) (2023), e7113.
[50] M.K. Koley, O.P. Chouhan, S. Biswas, J. Fernandes, A. Banerjee, A. Chattopadhyay, B. Varghese, P.T. Manoharan, A.P. Koley, Spectroscopic, electrochemical and DNA binding studies of some monomeric copper (II) complexes containing N_2S(thiolate)Cu core and N_4S(disulfide)Cu core, Inorg. Chim. Acta. 456 (2017) 179–198.
[51] O.A. El-Gammal, A.A. El-Bindary, F.Sh Mohamed, G.N. Rezk, M.A. El-Bindary, Synthesis, characterization, design, molecular docking, anti COVID-19 activity, DFT calculations of novel Schiff base with some transition metal complexes, J. Mol. Liq. 346 (2022), 117850.
[52] A.A. Frost, R.G. Pearson, Kinetics and Mechanisms, Wiley, New York, 1961.
[53] V. Chandrasekhar, R. Azhakar, G.T. Senthil Andavan, V. Krishnan, S. Zacchini, J.F. Bickley, P. Kögerler, A phosphorus supported multisite coordinating tris hydrazone P(S)[N(Me)N=CH-C_6H_4-*o*-OH]$_3$ as an efficient ligand for the assembly of trinuclear metal complexes: synthesis, structure, and magnetism, Inorg. Chem. 42 (2003) 5989–5998.
[54] A.E.M. Abdallah, S.A. Abdel-Latif, G.H. Elgemeie, Novel fluorescent benzothiazolyl-coumarin hybrids as anti-SARSCOVID-2 agents supported by molecular docking studies: design, synthesis, X-ray crystal structures, DFT, and TD-DFT/PCM calculations, ACS Omega 8 (22) (2023) 19587–19602.
[55] Z. Sanaei, G. Bahlakeh, B. Ramezanzadeh, M. Ramezanzadeh, Application of green molecules from *Chicory* aqueous extract for steel corrosion mitigation against chloride ions attack; the experimental examinations and electronic/atomic level computational studies, J. Mol. Liq. 290 (2019), 111176.
[56] S.A. Abdel-Latif, A.A. Mohamed, Novel Zn(II) complexes of 1,3-diphenyl-4-(arylazo) pyrazol-5-one derivatives: synthesis, spectroscopic properties, DFT calculations and first order nonlinear optical properties, J. Mol. Struct. 1156 (2018) 712–725.
[57] O.A. El-Gammal, F.Sh Mohamed, G.N. Rezk, A.A. El-Bindary, Structural characterization and biological activity of a new metal complexes based of Schiff base, J. Mol. Liq. 330 (2021), 115522.
[58] H.A. Kiwaan, A.S. El-Mowafy, A.A. El-Bindary, Synthesis, spectral characterization, DNA binding, catalytic and in vitro cytotoxicity of some metal complexes, J. Mol. Liq. 326 (2021), 115381.
[59] M.A. El-Bindary, A.A. El-Bindary, Synthesis, characterization, DNA binding, and biological action of dimedone arylhydrazone chelate, Appl. Organomet. Chem. 36 (4) (2022), e6576.
[60] R.S. Mulliken, Electronic Population analysis on LCAO-MO molecular wave functions, J. Chem. Phys. 23 (1955) 1833–1840.
[61] P. Politzer, D.G. Truhlar, Chemical Applications of Atomic and Molecular Electrostatic Potentials, Springer Science & Business Media, 2013.
[62] M.A. El-Bindary, M.G. El-Desouky, A.A. El-Bindary, Metal-organic frameworks encapsulated with an anticancer compound as drug delivery system: synthesis, characterization, antioxidant, anticancer, antibacterial and molecular docking investigation, Appl. Organomet. Chem. 36 (2022), e6660.
[63] X. Xiu, T. Feng, S.-S. Feng, W.-K. Dong, Influence of structural variation of salamo-based ligand on supramolecular architectures, Hirshfeld analyses, and fluorescence properties of new tetranuclear NiII complexes, Appl. Organomet. Chem. 35 (1) (2021), e6057.
[64] O.M.I. Adly, M. Shebl, E.M. Abdelrhman, B.A. El-Shetary Synthesis, spectroscopic, X-ray diffraction, antimicrobial and antitumor studies of Ni(II) and Co(II) complexes derived from 4-acetyl-5,6-diphenyl-3(2H)-pyridazinone and ethylenediamine, J. Mol. Struct. 1219 (2020), 128607.
[65] M. Shebl, O.M.I. Adly, H.F. El-Shafiy, S.M.E. Khalil, A. Taha, M.A.N. Mahdi, Structural variety of mono- and binuclear transition metal complexes of 3-[(2-hydroxy-benzylidene)-hydrazono]-1-(2-hydroxyphenyl)-butan-1-one: synthesis, spectral, thermal, molecular modeling, antimicrobial and antitumor studies, J. Mol. Struct. 1134 (2017) 649–660.
[66] A.Z. El-Sonbati, M.A. Diab, A.A. El-Bindary, M.I. Abou-Dobara, H.A. Seyam, Supramolecular coordination and antimicrobial activities of constructed mixed ligand complexes, Spectrochim. Acta 104 (2013) 213–221.
[67] M. Shebl, S.M.E. Khalil, M.A.A. Kishk, D.M. El-Mekkawi, M. Saif, New less toxic zeolite-encapsulated Cu(II) complex nanomaterial for dual applications in biomedical field and wastewater remediation, Appl. Organomet. Chem. 33 (2019) e5147.
[68] A.F. Shoair, A.A. El-Bindary, A.Z. El-Sonbati, R.M. Younes, Stereochemistry of new nitrogen containing heterocyclic aldehyde. VI. Novel structural and properties models of uranyl with quinoline azodyes, Spectrochim. Acta 57 (2001) 1683.
[69] A.W. Coats, J.P. Redfern, Reaction rate models for the thermal decomposition of ibuprofen crystals, Nature 20 (1964) 68–79.
[70] H.W. Horowitz, G. Metzger, Synthesis and characterization of some selenium nanometric compounds: spectroscopic, biological and antioxidant assessments, Anal. Chem. 35 (1963) 1464–1468.
[71] H. katouah, A. Sayqal, A.M. Al-Solimy, H.M. Abumelha, R. Shah, F. Alkhatib, S. Alzahrani, R. Zaky, N.M. El-Metwaly, Facile synthesis and deliberate characterization for new hydrazide complexes; cyclic voltammetry, crystal packing, eukaryotic DNA degradation and in-silico studies, J. Mol. Liq. 320 (2020), 114380.
[72] J.W. Moore, R.G. Pearson, Kinetics and Mechanism, John Wiley & Sons, 1961.
[73] A.F. Shoair, A.A. El-Bindary, N.A. El-Ghamaz, G.N. Rezk, Synthesis, characterization, DNA binding and antitumor activities of Cu(II) complexes, J. Mol. Liq. 269 (2018) 619–638.
[74] G.A.A. Al-Hazmi, K.S. Abou-Melha, I. Althagafi, N. El-Metwaly, F. Shaaban, M.S. Abdul Galil, A.A. El-Bindary, Synthesis and structural characterization of oxovanadium (IV) complexes of dimedone derivatives, Appl. Organomet. Chem. 34 (8) (2020), e5672.
[75] T.M.A. Al-Shboul, M. El-khateeb, Z.H. Obeidat, T.S. Ababneh, S.S. Al-Tarawneh, M.S. Al Zoubi, W. Alshaer, A. Abu Seni, T. Qasem, H. Moriyama, Y. Yoshida, H. Kitagawa, T.M.A. Jazzazi, Synthesis, characterization, computational and biological activity of some Schiff bases and their Fe, Cu and Zn complexes, INORGA 10 (8) (2022) 112.
[76] T.M. Radwan, M.A. El-Hashash, A.A.F. Wasfy, S.A. Abdallah, Antitumor, cytotoxic, and antioxidant evaluation of six heterocyclic compounds containing different heterocycle moieties, J. Heterocycl. Chem. 57 (3) (2020) 1111–1122.
[77] P.R. Ammal, A.R. Prasad, A. Joseph, Synthesis, characterization, in silico, and in vitro biological screening of coordination compounds with 1,2,4-triazine based biocompatible ligands and selected 3d-metal ions, Heliyon 6 (10) (2020), e05144.
[78] A. Singh, H.P. Gogoi, P. Barman, A.K. Guha, Novel thioether Schiff base transition metal complexes: design, synthesis, characterization, molecular docking, computational, biological and catalytic studies, Appl. Organomet. Chem. 36 (6) (2022), e6673.

[79] N.A.A. Elkanzi, H. Hrichi, H. Salah, M. Albqmi, A.M. Ali, A. Abdou, Synthesis, physicochemical properties, biological, molecular docking and DFT investigation of Fe(III), Co(II), Ni(II), Cu(II) and Zn(II) complexes of the 4-[(5-oxo-4,5-dihydro-1,3-thiazol-2-yl)hydrazono]methyl}phenyl 4-methylbenzenesulfonate Schiff-base ligand, Polyhedron 230 (2023), 116219.
[80] N.H. Mahmoud, G.H. Elsayed, A. Aboelnaga, A.M. Fahim, Spectroscopic studies, DFT calculations, cytotoxicity activity, and docking stimulation of novel metal complexes of Schiff base ligand of isonicotinohydrazide derivative, Appl. Organomet. Chem. 36 (7) (2022), e6697.
[81] M.M. Ghoneim, A.Z. El-Sonbati, A.A. El-Bindary, M.A. Diab, L.S. Serag, Polymer complexes. LX. Supramolecular coordination and structures of N(4-(acrylamido)-2-hydroxybenzoic acid) polymer complexes, Spectrochim. Acta 140 (2015) 111–131.
[82] A.A. El-Bindary, E.A. Toson, K.R. Shoueir, H.A. Aljohani, M.M. Abo-Ser, Metal–organic frameworks as efficient materials for drug delivery: synthesis, characterization, antioxidant, anticancer, antibacterial and molecular docking investigation, Appl. Organomet. Chem. 34 (2019), e5905.
[83] R.G. Deghadi, A.A. Abbas, G.G. Mohamed, Theoretical and experimental investigations of new bis (amino triazole) schiff base ligand: preparation of its UO2(II), Er(III), and La(III) complexes, studying of their antibacterial, anticancer, and molecular docking, Appl. Organomet. Chem. 35 (8) (2021), e6292.
[84] A.M. Abu-Dief, R.M. El-khatib, S.M. El Sayed, S. Alzahrani, F. Alkhatib, G. El-Sarrag, M. Ismael, Tailoring, structural elucidation, DFT calculation, DNA interaction and pharmaceutical applications of some aryl hydrazone Mn(II), Cu(II) and Fe(III) complexes, J. Mol. Struct. 1244 (2021), 131017.
[85] E.M. Abdelrhman, B.A. El-Shetary, M. Shebl, O.M.I. Adly, Coordinating behavior of hydrazone ligand bearing chromone moiety towards Cu(II) ions: synthesis, spectral, density functional theory (DFT) calculations, antitumor, and docking studies, Appl. Organomet. Chem. 35 (2021), e6183.